Mean-Square Radius of Gyration of Isotactic Oligo- and Poly(methyl methacrylate)s in Dilute Solution

Masanao Kamijo, Nobuo Sawatari, Toshiki Konishi, Takenao Yoshizaki, and Hiromi Yamakawa*

Department of Polymer Chemistry, Kyoto University, Kyoto 606-01, Japan

Received May 25, 1994; Revised Manuscript Received July 7, 1994®

ABSTRACT: The mean-square radius of gyration $\langle S^2 \rangle$ was determined by small-angle X-ray scattering and light scattering for 16 samples of isotactic oligo- and poly(methyl methacrylate)s (i-PMMA) in the range of weight-average molecular weight M_w from 4.58×10^2 (tetramer) to 1.71×10^6 in acetonitrile at 28.0 °C (Θ). The fraction of racemic diads f_r determined for them by ^{1}H NMR was ca. 0.01 independently of M_w except for the oligomers with very small M_w, for which it was somewhat larger. In contrast to the previous results for atactic (a-) PMMA with $f_r = 0.79$ in the unperturbed Θ state, for which the ratio $\langle S^2 \rangle / x_w$ as a function of the weight-average degree of polymerization x_w exhibits a maximum, it was found to increase monotonically with increasing x_w and level off to its asymptotic value for i-PMMA as in the case of atactic polystyrene (a-PS) with $f_r = 0.59$ previously studied. The data obtained were analyzed on the basis of the helical wormlike (HW) chain model to determine the model parameters. The results are $\lambda^{-1}\kappa_0 = 2.5$, $\lambda^{-1}\tau_0 = 1.3$, $\lambda^{-1} = 38.0$ Å, and $M_L = 32.5$ Å^{-1}, where κ_0 and τ_0 are the differential-geometrical curvature and torsion, respectively, of the characteristic helix taken at the minimum zero of the elastic energy of the model, λ^{-1} is the stiffness parameter, and M_L is the shift factor. The difference in local chain conformation between i- and a-PMMA is discussed in detail on the basis of the model parameters thus determined. It is then concluded that the above difference in the behavior of $\langle S^2 \rangle / x_w$ between i- and a-PMMA arises from the fact that the former is of weaker helical nature than the latter. In order to illustrate the situation, a picture is given of representative instantaneous contours of HW Monte Carlo chains for them and also for a-PS.

Introduction

In this series of experimental work[1] on dilute solutions of several kinds of flexible polymers and their oligomers in the unperturbed Θ state on the basis of the helical wormlike (HW) chain,[2,3] we have shown that their equilibrium conformational and steady-state transport properties depend substantially on the chain stiffness and local conformation and cannot be completely explained by the Gaussian chain model. On the other hand, the rotational isomeric state (RIS) model[4] predicts that the unperturbed dimensions of asymmetric polymer chains depend appreciably on the stereochemical composition (the fraction of racemic diads f_r). Naturally, their other dilute solution properties may also be regarded as dependent on f_r. In the course of these studies made so far, we have therefore taken special care of the regulation of f_r of the samples used in the case of asymmetric polymers, i.e., polystyrene (PS) and poly(methyl methacrylate) (PMMA).

Despite the obvious fact above, however, experimental investigations have not yet been performed systematically and extensively on the f_r dependence of solution properties of asymmetric polymers over a wide range of molecular weight, including the oligomers. Thus, in the present and forthcoming papers, we do this by taking PMMA as an example. Specifically, we carry out measurements of the mean-square radius of gyration $\langle S^2 \rangle$, intrinsic viscosity, translational diffusion coefficient, and so on for unperturbed isotactic (i-) PMMA with $f_r \simeq 0$ and compare the results with the corresponding previous ones for atactic (a-) PMMA[5-9] with $f_r = 0.79$ on the basis of the HW model.

Of course, PS is an alternative, interesting and important polymer in this sense, and both isotactic and syndiotactic samples are available for it. As is well-known, however, there are not suitable poor solvents that realize the Θ temperatures for them at room temperature, so it is difficult to obtain accurate data for them. On the other hand, this is not the case with PMMA. In anticipation of the results, we note that acetonitrile is a Θ solvent for i-PMMA as well as for a-PMMA (Θ = 44.0 °C for the later[5]), although the Θ temperatures are somewhat different. Thus, in this paper, we make a study of $\langle S^2 \rangle$ for i-PMMA in acetonitrile as a first step.

Experimental Section

Materials. The i-PMMA samples with weight-average molecular weights $M_w \lesssim 4 \times 10^4$, including the oligomers, were prepared by living anionic polymerization, following the procedure of Ute et al.[10] The polymerization was carried out in toluene at −78 °C with *t*-C_4H_9MgBr as an initiator prepared in diethyl ether. It was terminated by adding a solution of phenol in toluene after the reaction had proceeded for ca. 20 min for $M_w \lesssim 10^3$, ca. 2 days for $10^3 \lesssim M_w \lesssim 10^4$, and ca. 6 days for $M_w \gtrsim 10^4$. The initiating chain-end group of the original i-PMMA samples thus obtained is *tert*-butyl and the other end is a hydrogen atom. The samples with $M_w \gtrsim 4 \times 10^4$ were fractions separated from a commercial sample 9011-14-7 from Scientific Polymer Products, Inc.

The original synthesized and commercial samples were separated into fractions by preparative gel permeation chromatography (GPC) for the test samples with $M_w \lesssim 10^3$ and by fractional precipitation using 1-propanol and benzene as a solvent for those with $M_w \lesssim 2 \times 10^3$ and $M_w \gtrsim 2 \times 10^3$, respectively, and hexane as a precipitant.

The samples with $M_w \lesssim 10^3$ were dissolved in benzene, then filtered through a Teflon membrane of pore size 0.45 μm, and finally dried in a vacuum at 40–60 °C for 2–14 days. The samples with $M_w \gtrsim 10^3$ were freeze-dried from their benzene solutions after filtration through a membrane of the same kind.

The solvents acetonitrile used for light scattering (LS) and small-angle X-ray scattering (SAXS) measurements and acetone used for LS measurements were purified according to standard procedures. The solvent used for NMR spectroscopy was of reagent grade.

^{1}H NMR. ^{1}H NMR spectra for some of the i-PMMA samples were recorded on a JEOL JMN GX-400 spectrometer at 399.8 MHz. The spectrum was taken in deuterated chloroform containing tetramethylsilane as an internal standard at 35–55

® Abstract published in *Advance ACS Abstracts*, September 1, 1994.

0024-9297/94/2227-5697$04.50/0

°C using an rf pulse angle of 90° with a pulse repetition time of 56 s for the oligomer samples and of 26 s for the samples with $M_w \gtrsim 10^4$.

Light Scattering. LS measurements were carried out to determine M_w of the samples with $M_w > 10^3$, the Θ temperature of acetonitrile solutions, and $\langle S^2 \rangle$ for the samples with $M_w > 3 \times 10^5$. M_w was determined in acetonitrile at Θ, and for a few samples also in acetone at 25.0 °C. (We carried out the measurements in acetone to compare the results for M_w with those in acetonitrile.) For the determination of Θ, the second virial coefficient A_2 was measured for three samples at several temperatures ranging from 23 to 35 °C.

A Fica 50 light scattering photometer was used for all the measurements with vertically polarized incident light of wavelength 436 nm. For a calibration of the apparatus, the intensity of light scattered from pure benzene was measured at a scattering angle of 90° at 25.0 °C, where the Rayleigh ratio R_{Uu} (90°) of pure benzene was taken as 46.5×10^{-6} cm^{-1}. The depolarization ratio ρ_u of pure benzene at 25.0 °C was determined to be 0.41 ± 0.01 by the method of Rubingh and Yu.[11] Scattering intensities were measured at five different concentrations and at scattering angles ranging from 30 to 150°. The data obtained were treated by the Berry square-root plot.[12] In the present case, corrections for the optical anisotropy were unnecessary for $M_w \gtrsim 3 \times 10^3$ since the degree of depolarization was negligibly small. For $10^3 \lesssim M_w \lesssim 3 \times 10^3$, measurements with unpolarized incident light were also carried out to make corrections for the optical anisotropy.

The most concentrated solution of each sample was prepared gravimetrically and made homogeneous by continuous stirring at 50 °C for 2 days. It was optically purified by filtration through a Teflon membrane of pore size 0.45 μm. The solutions of lower concentrations were obtained by successive dilution. The weight concentrations of the test solutions were converted to the polymer mass concentrations c by the use of the density of the solvent.

The refractive index increment $\partial n/\partial c$ was measured at 436 nm by the use of a Shimadzu differential refractometer for some samples in acetonitrile at 28.0 °C and in acetone at 25.0 °C. For the acetonitrile solutions, $\partial n/\partial c$ was found to be 0.133_5, 0.142_0, and 0.144_9 cm^3/g for $M_w = 1.01 \times 10^3$, 1.79×10^3, and 3.12×10^3, respectively, and to become constant for larger M_w. The result for the acetone solution was 0.138_0 cm^3/g for $M_w \gtrsim 3 \times 10^5$.

Small-Angle X-ray Scattering. SAXS measurements were carried out for 11 samples with $M_w \lesssim 7 \times 10^4$ in acetonitrile at 28.0 °C by the use of an Anton Paar Kratky U-slit camera with an incident X-ray of wavelength 1.54 Å (Cu Kα line). The apparatus system and the methods of data acquisition and analysis are the same as those described in the previous paper.[13]

The measurements were performed for four or five solutions of different concentrations for each polymer sample and for the solvent at scattering angles ranging from 1×10^{-3} rad to a value at which the scattering intensity was negligibly small. Corrections for the stability of the X-ray source and the detector electronics were made by measuring the intensity scattered from Lupolene (a platelet of polyethylene) used as a working standard before and after each measurement for a given sample solution and the solvent. The effect of absorption of X-rays by a given solution or the solvent was also corrected by measuring the intensity scattered from Lupolene with insertion of the solution or solvent between the X-ray source and Lupolene. The degree of absorption increased linearly with increasing solute concentration.

The excess reduced scattering intensity $\Delta I_R(k)$ as a function of the magnitude k of the scattering vector was determined from the observed (smeared) excess reduced intensity by the modified Glatter desmearing method, which consists of expressing the true scattering function in terms of cubic B-spline functions, as described before.[13] Here, k is given by

$$k = (4\pi/\lambda_0) \sin(\theta/2) \quad (1)$$

with λ_0 the wavelength of the incident X-ray and θ the scattering angle. All the data were processed by the use of a Fujitsu M-1800/30 digital computer at this university. Then the data for $\Delta I_R(k)$ were analyzed by using the Berry square-root plot[12] to evaluate the apparent mean-square radius of gyration $\langle S^2 \rangle_s$.[13]

The test solutions were prepared gravimetrically, and their polymer mass concentrations c were calculated from the weight fractions by using the densities of the respective solutions. The densities of the solvent and solutions were measured with a pycnometer of the Lipkin–Davison type.

Table 1. Values of M_w, x_w, and M_w/M_n for Isotactic Oligo- and Poly(methyl methacrylate)s

sample	M_w	x_w	M_w/M_n
iOM4	4.58×10^2	4	1.00
iOM5	5.58×10^2	5	1.00
iOM6	6.58×10^2	6	1.00
iOM7	7.89×10^2	7.31	1.01
iOM10	1.01×10^3	9.52	1.02
iOM18	1.79×10^3	17.3	1.10
iOM31	3.12×10^3	30.6	1.04
iMM1	1.07×10^4	106	1.05
iMM2	2.57×10^4	256	1.07
iMM3	3.06×10^4	305	1.06
iMMc7	7.01×10^4	700	1.06
iMMc30	3.13×10^5 (3.16×10^5)[a]	3130	1.08
iMMc60	5.82×10^5	5820	1.06
iMMc90	9.46×10^5	9460	1.09
iMMc100	9.61×10^5	9610	1.08
iMMc170	1.71×10^6 (1.62×10^6)	17100	1.09

[a] The figures in parentheses represent the values in acetone.

Results

Molecular Weights and Stereochemical Composition. The values of M_w, the weight-average degree of polymerization x_w, and the ratio of M_w to the number-average molecular weight M_n determined for the i-PMMA samples we used for the measurements of $\langle S^2 \rangle$ are given in Table 1. The sample code iMMcx indicates that the sample is a fraction separated from the commercial sample, and all the other samples are those from the original samples synthesized in the present study. Note that the samples iOM3 (trimer) and iMMc4 ($M_w = 3.68 \times 10^4$), which were used only for the determination of f_r, and also the sample iMMc50′ ($M_w = 5.25 \times 10^5$), which was used only for the determination of Θ, are omitted in the table. From analytical GPC, the four oligomer samples iOM3 through iOM6 were found to be completely monodisperse. The samples iOM3 and iOM4 were confirmed to be the trimer and tetramer, respectively, by ^{1}H NMR spectroscopy, as shown later, and the samples iOM5 and iOM6 were confirmed to be the pentamer and hexamer, respectively, by analytical GPC. The oligomer sample iOM7 was also identified by analytical GPC, but it was found to contain the octamer by 30.8 wt %. For this oligomer sample, the values of M_w and M_n were calculated from its molecular weight distribution thus determined.

For the other samples with $M_w > 10^3$, the values of M_w were determined from LS measurements, and those of M_w/M_n, from analytical GPC. The figures in parentheses in Table 1 represent the values of M_w determined in acetone, which are in good agreement with those in acetonitrile. This indicates that the possible molecular association in acetonitrile[14] does not occur at least in dilute solution at 28.0 °C.

Figure 1a shows a ^{1}H NMR spectrum of methylene and methine protons of the sample iOM3 as an example. The assignments of the peaks to the six methylene protons and one (7th) methine proton of the four kinds of stereochemical isomers, i.e., mm, mr, rm, and rr (from the initiating end to the terminating one) with m and r indicating the meso and racemic diads, respectively, have been made on the basis of the ^{1}H NMR spectra obtained by Ute et al.[15] for the four isomers. The assignments are indicated by the symbol $x\alpha\beta$ in the spectrum, where x (=1–7) is the proton number and α, β = m, r. From the

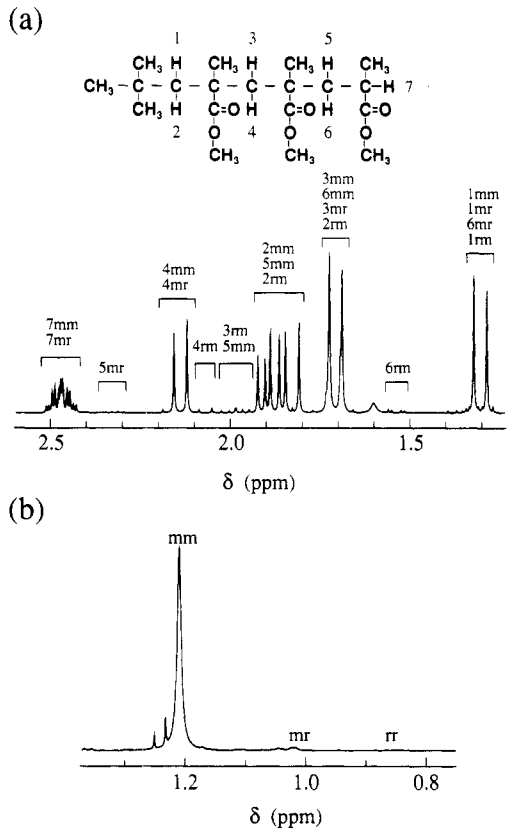

Figure 1. ^{1}H NMR spectra of methylene and methine protons of the sample iOM3 (a) and α-methyl protons of the sample iMMc4 (b).

Table 2. Values of f_r Determined from ^{1}H NMR Spectra

sample	f_r	sample	f_r
iOM3	0.06_5	iMMc4	0.01_5
iOM4	0.05_0	iMMc	0.00_7
iMM1	0.02_2		

relative intensities of these peaks, some of which cannot be distinguished, the (mole) fractions of the four isomers may be evaluated. The results are mm:mr:rm:rr = 87:9:4:0, and then f_r is evaluated to be 0.06_5 for the sample iOM3. We note that the diad distribution in this sample is not Bernoullian. The value of f_r for the sample iOM4 was also determined in the same manner on the basis of the ^{1}H NMR spectra obtained by Ute et al.[16] for the eight isomers, although our spectrum is omitted here. From these ^{1}H NMR spectra, the samples iOM3 and iOM4 have been confirmed to be the trimer and tetramer, respectively.

Similarly, Figure 1b shows a ^{1}H NMR spectrum of α-methyl protons of the sample iMMc4. In this case, the assignments of the peaks to the three kinds of triads, i.e., mm, mr, and rr, have been made on the basis of the ^{1}H NMR spectra obtained by Chûjô et al.[17] for PMMA, as shown in the figure. The relative intensities of the three peaks for mm, mr, and rr are 0.97_7, 0.01_7, and 0.00_6, respectively, and f_r is evaluated to be 0.01_5 from these values, assuming that the triad distribution in the sample is Bernoullian as in the case of a-PMMA.[5] The values of f_r for the sample iMM1 and the original commercial sample, which we simply designate by iMMc, were also determined in the same manner.

The values of f_r thus determined for the samples iOM3, iOM4, iMM1, iMMc4, and iMMc are given in Table 2. It is seen that f_r is ca. 0.01 independently of M_w except for the oligomers with very small M_w. There is some deviation of the stereoregularity at the chain ends, which may be regarded as arising from a kind of end effect.

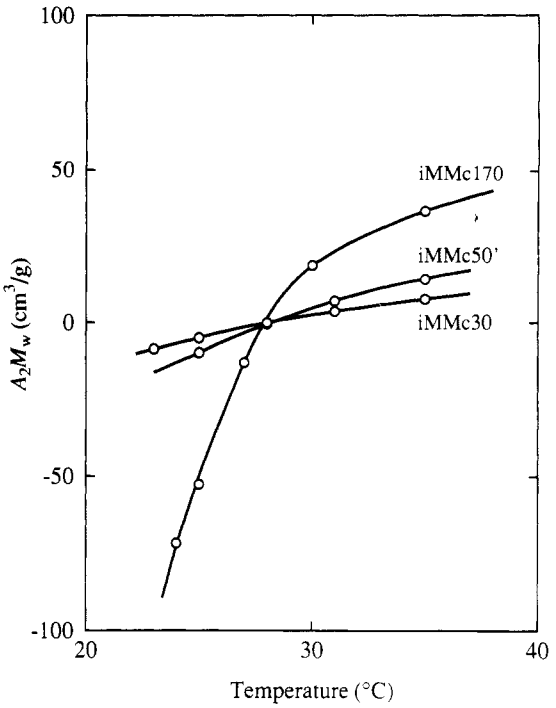

Figure 2. Plots of A_2M_w against temperature for the i-PMMA samples indicated in acetonitrile.

Θ Temperature. Figure 2 shows plots of A_2M_w against temperature for the three samples iMMc30, iMMc50′, and iMMc170 in acetonitrile. It is seen from the figure that A_2 vanishes at almost the same temperature independent of M_w, leading to the conclusion that the Θ temperature is 28.0 °C for solutions of i-PMMA with $f_r \simeq 0.01$ in acetonitrile. This value of Θ is in rather good agreement with the value 27.6 °C determined by Krause and Cohn-Ginsberg,[18] although their i-PMMA samples are considered to have f_r equal to 0.1–0.2 and somewhat larger than the present values.

Mean-Square Radii of Gyration $\langle S^2\rangle_s$ and $\langle S^2\rangle$. The values of $(c/\Delta I_R)^{1/2}_{k=0}$ and $(c/\Delta I_R)^{1/2}_{c=0}$ for all the samples with $M_w < 10^5$ listed in Table 1 in acetonitrile at 28.0 °C (Θ) were determined by extrapolation to zero angle and zero concentration, respectively, from the SAXS data for $(c/\Delta I_R)^{1/2}$ obtained at finite scattering angles and concentrations. Figures 3 and 4 show plots of $(Kc/\Delta I_R)^{1/2}_{k=0}$ against c and those of $(Kc/\Delta I_R)^{1/2}_{c=0}$ against k^2, respectively, where K is the optical constant which depends on the SAXS apparatus (and also the cell) used. Since we used a new SAXS cell for the present measurements, the value of K previously determined[13] could not be adopted. Thus, in the figures, we have used its proper value for each sample so that the value of the common intercept $(Kc/\Delta I_R)^{1/2}_{c=0,k=0}$ at $c = 0$ and $k = 0$ may be consistent with the value of M_w determined from LS measurements and given in Table 1, for convenience. Note that it may be related to M_w as follows

$$(Kc/\Delta I_R)^{1/2}_{c=0,k=0} = M_w^{-1/2} \qquad (2)$$

and also that the choice of K does not affect the determination of $\langle S^2\rangle$.

In Figure 3, the straight line fitted to the data points for each oligomer sample has definitely a positive slope, indicating that A_2 does not vanish for i-PMMA oligomers even in the unperturbed Θ state, i.e., at the Θ temperature at which A_2 vanishes for large M_w ($\gtrsim 10^5$). This is the same behavior as found for the SAXS data for the a-PS[13] and

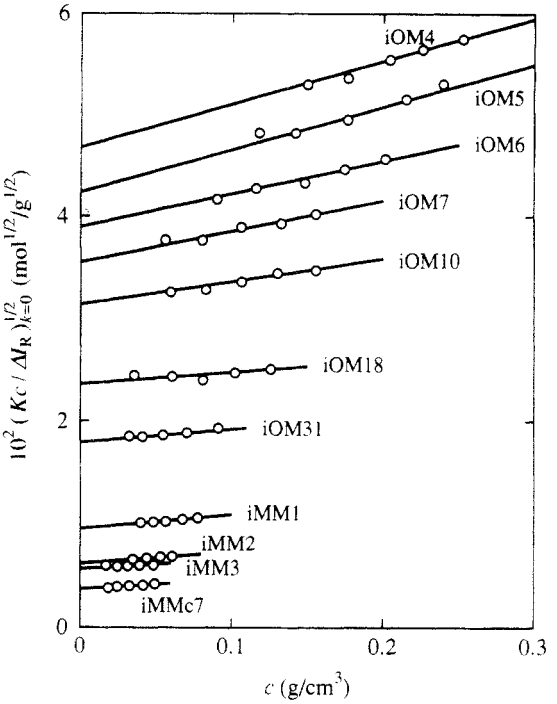

Figure 3. Plots of $(Kc/\Delta I_R)_{k=0}^{1/2}$ against c for the i-PMMA samples indicated in acetonitrile at 28.0 °C.

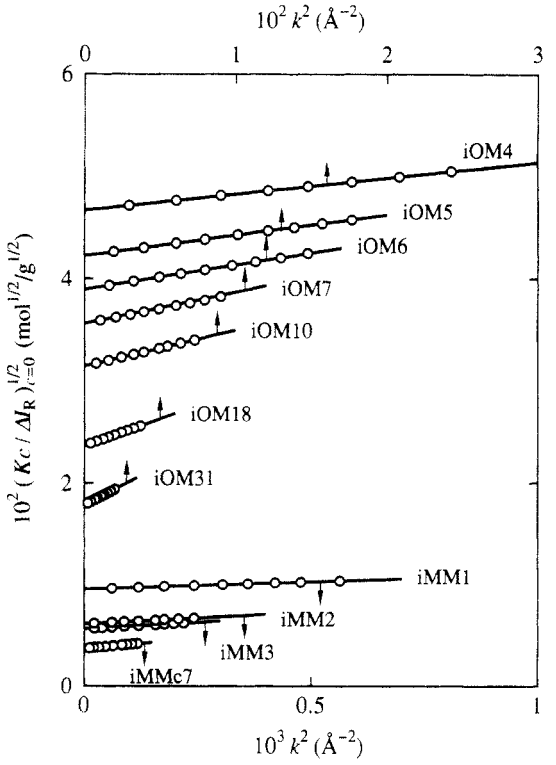

Figure 4. Plots of $(Kc/\Delta I_R)_{c=0}^{1/2}$ against k^2 for the i-PMMA samples indicated in acetonitrile at 28.0 °C.

a-PMMA[5] oligomers at the respective Θ temperatures. As noted in the previous LS study of A_2 of a-PMMA,[19] SAXS data are not accurate enough to deduce a quantitative conclusion, so that we do not further discuss the results.

In Figure 4, the data points for each sample also follow the indicated straight line in the range of k^2 displayed, thereby permitting an accurate determination of the (apparent) mean-square radius of gyration $\langle S^2\rangle_s$ from the ratio of its slope to its intercept.[13] The valeus of $\langle S^2\rangle_s^{1/2}$ thus determined are listed in the second column of Table 3. As discussed previously,[13] the values of $\langle S^2\rangle_s$ contain

Table 3. Results of SAXS Measurements on Isotactic Oligo- and Poly(methyl methacrylate)s in Acetonitrile at 28.0 °C

sample	$\langle S^2\rangle_s^{1/2}$, Å	$\langle S^2\rangle^{1/2}$, Å
iOM4	4.4_8	3.4_5
iOM5	5.2_9	4.4_5
iOM6	6.1_1	5.3_9
iOM7	7.0_1	6.4_0
iOM10	8.1_1	7.5_9
iOM18	$11._6$	$11._2$
iOM31	$15._9$	$15._6$
iMM1	$30._0$	$29._9$
iMM2	$47._3$	$47._2$
iMM3	$52._3$	$52._2$
iMMc7	$79._4$	$79._4$

Table 4. Results of LS Measurements on Isotactic Poly(methyl methacrylate) in Acetonitrile at 28.0 °C

sample	$10^{-5}M_w$	$10^{-2}\langle S^2\rangle^{1/2}$, Å
iMMc30	3.13	1.7_0
iMMc60	5.82	2.3_1
iMMc90	9.46	3.0_0
iMMc100	9.61	3.0_2
iMMc170	17.1	3.9_8

contributions from the finite cross section of the polymer chain due to the electron distribution. Thus a correction must be made to separate $\langle S^2\rangle$ itself of the chain contour from $\langle S^2\rangle_s$, since for the former a theoretical expression has been derived to be compared with experiment. For this purpose, we may use the equation

$$\langle S^2\rangle_s = \langle S^2\rangle + S_c^2 \tag{3}$$

which has been derived for a continuous chain having a uniform circular cross section with S_c being the radius of gyration of the cross section.[13]

As in the case of the a-PMMA previously studied,[5] we make the correction by adopting the value 8.2 Å^2 for S_c^2 calculated from the relation $S_c^2 = \upsilon_2 M_L/2\pi N_A$ with N_A the Avogadro number, υ_2 the partial specific volume of the polymer, and M_L the shift factor as defined as the molecular weight per unit contour length of the polymer chain, where we have used the value 0.81 cm^3/g of υ_2 for the i-PMMA sample with sufficiently large M_w and the value 38.6 Å^{-1} of M_L corresponding to its chain fully extended to the all-trans conformation[20] as in the case of a-PMMA.[5] The results for $\langle S^2\rangle^{1/2}$ thus obtained are given in the third column of Table 3. For i-PMMA, $\langle S^2\rangle_s$ is seen to become equal to $\langle S^2\rangle$ for $M_w \gtrsim 10^4$.

Table 4 summarizes the results obtained for $\langle S^2\rangle^{1/2}$ from LS measurements for the samples with $M_w \gtrsim 3 \times 10^5$ in acetonitrile at 28.0 °C (Θ) along with those for M_w.

Molecular Weight Dependence of $\langle S^2\rangle_s/M_w$. Figure 5 shows plots of the ratio $\langle S^2\rangle_s/M_w$ against log M_w with the present data for i-PMMA with $f_r \simeq 0.01$ in acetonitrile at 28.0 °C (Θ) (unfilled circles). For comparison, it also includes the previous data for a-PMMA with $f_r = 0.79$ in acetonitrile at 44.0 °C (Θ)[5,21] (filled circles). Both of them were obtained from SAXS for $M_w \lesssim 2 \times 10^5$ and from LS for $M_w \gtrsim 2 \times 10^5$. The SAXS data for i-PMMA are smoothly joined to the corresponding LS data, the latter being almost independent of M_w, as in the case of a-PMMA; the solid curves connect the data points smoothly. As noted in the previous paper,[5] as M_w is increased, the ratio $\langle S^2\rangle_s/M_w$ for a-PMMA first increases for $M_w \lesssim 10^3$, then passes through a maximum at $M_w \simeq 3 \times 10^3$, and finally approaches its asymptotic value for $M_w \gtrsim 10^5$. In contrast to this, the ratio for i-PMMA increases monotonically with increasing M_w and levels off to its asymptotic value for M_w

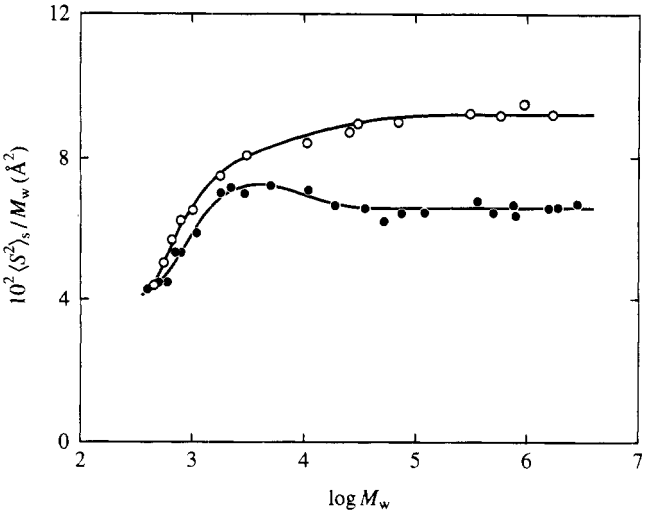

Figure 5. Molecular weight dependence of $\langle S^2\rangle_s/M_w$: (○) present data for i-PMMA with $f_r \simeq 0.01$ in acetonitrile at 28.0 °C; (●) previous data for a-PMMA with $f_r = 0.79$ in acetonitrile at 44.0 °C.[5,21] The solid curves connect the data points smoothly.

$\gtrsim 3 \times 10^4$, which is appreciably larger than that for a-PMMA. The difference between the data for the two polymers becomes large for M_w larger than the value ($\sim 3 \times 10^3$) corresponding to the maximum ratio for a-PMMA.

Discussion

HW Model Parameters. The HW chain[2,3] may be described in terms of four basic model parameters: the differential-geometrical curvature κ_0 and torsion τ_0 of its characteristic helix taken at the minimum zero of its elastic energy, the static stiffness parameter λ^{-1}, and the shift factor M_L.

Now, for the HW chain of total contour length L, $\langle S^2\rangle$ may be given by[3,22]

$$\langle S^2\rangle = \lambda^{-2} f_S(\lambda L; \lambda^{-1}\kappa_0, \lambda^{-1}\tau_0) \tag{4}$$

where the function f_S is defined by

$$f_S(L; \kappa_0, \tau_0) = \frac{\tau_0^2}{\nu^2} f_{S,KP}(L) + \frac{\kappa_0^2}{\nu^2}\left[\frac{L}{3r}\cos\varphi - \frac{1}{r^2}\cos(2\varphi) + \frac{2}{r^3 L}\cos(3\varphi) - \frac{2}{r^4 L^2}\cos(4\varphi) + \frac{2}{r^4 L^2}e^{-2L}\cos(\nu L + 4\varphi)\right] \tag{5}$$

with

$$\nu = (\kappa_0^2 + \tau_0^2)^{1/2} \tag{6}$$

$$r = (4 + \nu^2)^{1/2} \tag{7}$$

$$\varphi = \cos^{-1}(2/r) \tag{8}$$

and with $f_{S,KP}$ being the function f_S for the Kratky–Porod (KP) wormlike chain[23] and being given by

$$f_{S,KP}(L) = \frac{L}{6} - \frac{1}{4} + \frac{1}{4L} - \frac{1}{8L^2}(1 - e^{-2L}) \tag{9}$$

In the limit of $\lambda L \to \infty$, we have

$$\lim_{\lambda L\to\infty} f_S(\lambda L)/\lambda L = c_\infty/6 \tag{10}$$

with

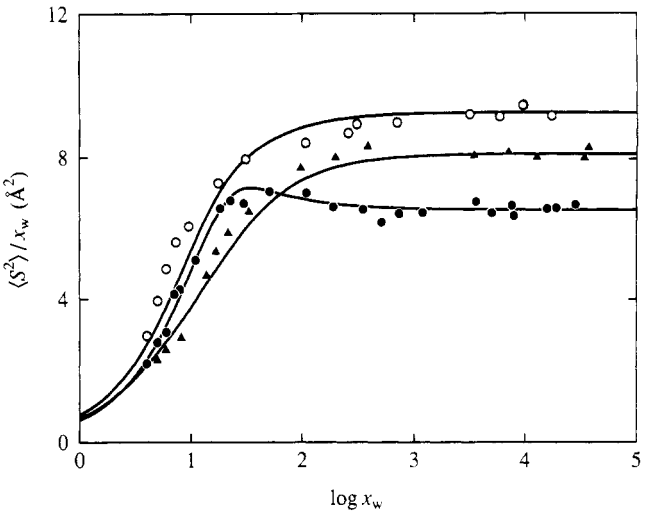

Figure 6. Plots of $\langle S^2\rangle/x_w$ against log x_w: (○) present data for i-PMMA with $f_r \simeq 0.01$ in acetonitrile at 28.0 °C; (●) previous data for a-PMMA with $f_r = 0.79$ in acetonitrile at 44.0 °C;[5,21] (▲) previous data for a-PS with $f_r = 0.59$ in cyclohexane at 34.5 °C.[13,24] The solid curves represent the respective best fit HW theoretical values calculated with the model parameters listed in Table 5.

$$c_\infty = \frac{4 + (\lambda^{-1}\tau_0)^2}{4 + (\lambda^{-1}\kappa_0)^2 + (\lambda^{-1}\tau_0)^2} \tag{11}$$

If x is the degree of polymerization of a given real chain, then $\langle S^2\rangle/x$ and x are related to $f_S(\lambda L)$ and L by the equations

$$\langle S^2\rangle/x = (M_0\lambda^{-1}/M_L)[f_S(\lambda L; \lambda^{-1}\kappa_0, \lambda^{-1}\tau_0)/\lambda L] \tag{12}$$

and

$$\log x = \log(\lambda L) + \log(\lambda^{-1} M_L/M_0) \tag{13}$$

respectively, with M_0 the molecular weight of its repeat unit. From eqs 10 and 12, we have

$$\lim_{x\to\infty}\langle S^2\rangle/x = M_0\lambda^{-1}c_\infty/6M_L \tag{14}$$

Figure 6 shows plots of $\langle S^2\rangle/x_w$ against log x_w with the present data for i-PMMA with $f_r \simeq 0.01$ in acetonitrile at 28.0 °C (Θ) (unfilled circles). For comparison, it also includes the previous data for a-PMMA with $f_r = 0.79$ in acetonitrile at 44.0 °C (Θ)[5,21] (filled circles) and for a-PS with $f_r = 0.59$ in cyclohexane at 34.5 °C (Θ)[13,24] (filled triangles). The solid curves represent the respective best fit HW theoretical values calculated from eqs 4–9 with the values of the model parameters listed in Table 5. The theoretical curve for i-PMMA may reproduce well the experimental values as in the cases of a-PMMA and a-PS.

It is clearly seen from Figure 6 and the values of λ^{-1} in the sixth column of Table 5 that the asymptotic value of $\langle S^2\rangle/x_w$ in the limit of $x_w \to \infty$, which is equal to 9.3_1, 6.5_7, and 8.1_3 Å^2 for i-PMMA, a-PMMA,[21] and a-PS,[24] respectively, cannot be correlated directly to the chain stiffness (λ^{-1}). It is important to note that the asymptotic value is related to the Kuhn statistical segment length A_K and the persistence length q, which are defined by

$$A_K \equiv \lim_{L\to\infty}\langle R^2\rangle/L \ (\leq\lambda^{-1}) \tag{15}$$

$$q \equiv \lim_{L\to\infty}\langle \mathbf{R}\cdot\mathbf{u}_0\rangle \tag{16}$$

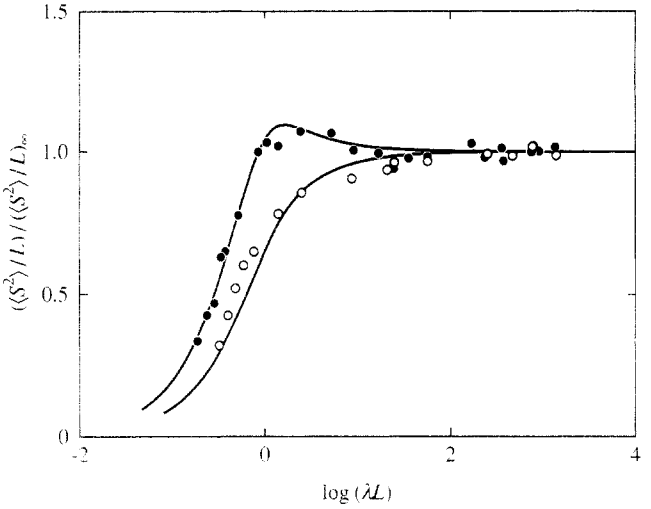

Figure 7. Plots of $(\langle S^2\rangle/L)/(\langle S^2\rangle/L)_\infty$ against $\log(\lambda L)$: (○) present data for i-PMMA with $f_r \simeq 0.01$ in acetonitrile at 28.0 °C; (●) previous data for a-PMMA with $f_r = 0.79$ in acetonitrile at 44.0 °C.[5,21] The solid curves represent the respective best fit HW theoretical values calculated with the model parameters listed in Table 5.

Table 5. Values of the HW Model Parameters

polymer (f_r)	solvent	temp, °C	$\lambda^{-1}\kappa_0$	$\lambda^{-1}\tau_0$	λ^{-1}, Å	M_L, Å^{-1}
i-PMMA (0.01)	acetonitrile	28.0	2.5	1.3	38.0	32.5
a-PMMA (0.79)	acetonitrile	44.0	4.0	1.1	57.9	36.3
a-PS (0.59)	cyclohexane	34.5	3.0	6.0	20.6	35.8

respectively, by the equation[3]

$$A_K = 2q = (6M_L/M_0)\lim_{x\to\infty}\langle S^2\rangle/x \qquad (17)$$

where **R** is the end-to-end vector of the chain, $\mathbf{u}_0$ is its initial unit tangent vector, and $\langle\ \rangle$ denotes an unperturbed average. Then, for polymer chains having the same ratio M_L/M_0, A_K is proportional to the asymptotic value of $\langle S^2\rangle/x$. Therefore, the above results confirm that A_K (and q) cannot in general be a measure of chain stiffness[3] (and the characteristic ratio, C_∞,[4] is not so either) since the values of M_L/M_0 are close to each other for these three polymers. (Note that $A_K = \lambda^{-1}$ for the KP chain.[3])

It must also be noted here that the value of M_L for i-PMMA is somewhat smaller than that for a-PMMA and also that for a-PS (with almost the same M_0). A similar result has been obtained in the previous analysis of RIS data for the persistence vector,[25] but the reason for this is not yet clear.

Local Chain Conformations. In this subsection, we discuss the local chain conformation on the basis of the HW model parameters κ_0, τ_0, and λ^{-1}. In the previous study of $\langle S^2\rangle$ of a-PMMA,[5] we have already made rather in detail a comparison between the local conformations of a-PMMA and a-PS chains in this way. Thus our major attention is given to the dependence on f_r of the local conformation of PMMA chains pictured in a similar fashion.

Before proceeding to do this, we examine the difference in the overall behavior of $\langle S^2\rangle$ between i- and a-PMMA. For this purpose, it is convenient to plot the ratio $(\langle S^2\rangle/L)/(\langle S^2\rangle/L)_\infty$ against $\log(\lambda L)$, where $(\langle S^2\rangle/L)_\infty$ denotes the asymptotic value of the ratio $\langle S^2\rangle/L$ in the limit of $L \to \infty$. Figure 7 shows such plots with the same data as those in Figure 6 for i-PMMA (unfilled circles) and a-PMMA (filled circles), where we have used eq 13 to calculate λL. The solid curves represent the respective best fit HW theoretical values calculated as in the last subsection (using eq 13). It is seen that the shoulder part of the curve is more square for a-PMMA than for i-PMMA, it exhibiting a maximum for the former, and that the curve is always lower for the latter than for the former except at large λL. (The curve for a-PS is even lower, although we do not show the results explicitly because of their complexity.) This difference in the behavior of the ratio $(\langle S^2\rangle/L)/(\langle S^2\rangle/L)_\infty$ may be considered to reflect directly the differences in stiffness and local conformation between the PMMA chains with different f_r. Thus it is concluded that in our HW language,[26] the *helical nature* is stronger for the a-PMMA chain than for the i-PMMA chain (see Figure 2 of ref 26).

Table 6. Values of the Characteristic Helix Parameters

polymer (f_r)	solvent	temp, °C	ρ, Å	h, Å
i-PMMA (0.01)	acetonitrile	28.0	12.0	39.1
a-PMMA (0.79)	acetonitrile	44.0	13.5	23.3
a-PS (0.59)	cyclohexane	34.5	1.37	17.3

Now, according to the HW model, a flexible polymer chain in dilute solution may be pictured as a regular helix (i.e., the characteristic helix) disturbed (or destroyed) by thermal fluctuations or a random coil retaining more or less helical portions. The shape of the characteristic helix may be determined as a space curve by the radius ρ and pitch h, which may be written in terms of κ_0 and τ_0 as

$$\rho = \kappa_0/(\kappa_0^2 + \tau_0^2) \qquad (18)$$

$$h = 2\pi\tau_0/(\kappa_0^2 + \tau_0^2) \qquad (19)$$

and the degree of disturbance (thermal fluctuation) may be represented by the parameter λ ($=k_BT/2\epsilon$ with k_B the Boltzmann constant, T the absolute temperature, and ϵ the bending force constant), so that the regular helical structure is destroyed to a less extent in the chain with larger stiffness λ^{-1}. In general, the chain of strong helical nature has large ρ (compared to h) and large λ^{-1}, and thus retains rather large and clearly distinguishable helical portions in dilute solution. Note that the chain with vanishing ρ (i.e., the KP chain) has no helical nature irrespective of the value of λ^{-1} since its characteristic helix becomes a straight line (rod) and that the chain with small λ^{-1} is not of strong helical nature irrespective of the shape of its characteristic helix.

In Table 6 are given the values of ρ and h calculated for the i- and a-PMMA chains and also for the a-PS chain from eqs 18 and 19 with the values of $\lambda^{-1}\kappa_0$, $\lambda^{-1}\tau_0$, and λ^{-1} given in Table 5. We note that the values of ρ and h for a-PS given in the table are somewhat smaller than the previous values[5] because of the minor changes[24] of the values of the model parameters λ^{-1} and M_L. The values of ρ for the i- and a-PMMA chains are nearly equal to each other, while h is larger for the former than for the latter, the characteristic helix being more extended for the former. Also from this result and the fact that λ^{-1} is larger for the a-PMMA chain, it is concluded that a-PMMA is of stronger helical nature than the i-PMMA chain. As for the a-PS chain, note that its characteristic helix is more extended (closer to a straight line) than that of the i-PMMA and its λ^{-1} is the smallest, so that it is of the weakest helical nature of the three chains.

In order to make such differences in local chain conformation between these chains more visual, we have generated HW Monte Carlo chains[5] corresponding to the i- and a-PMMA and also to the a-PS, each with $x = 500$. Note that for this value of x (x_w), their $\langle S^2\rangle/x_w$ values already reach nearly the respective asymptotic ones. The

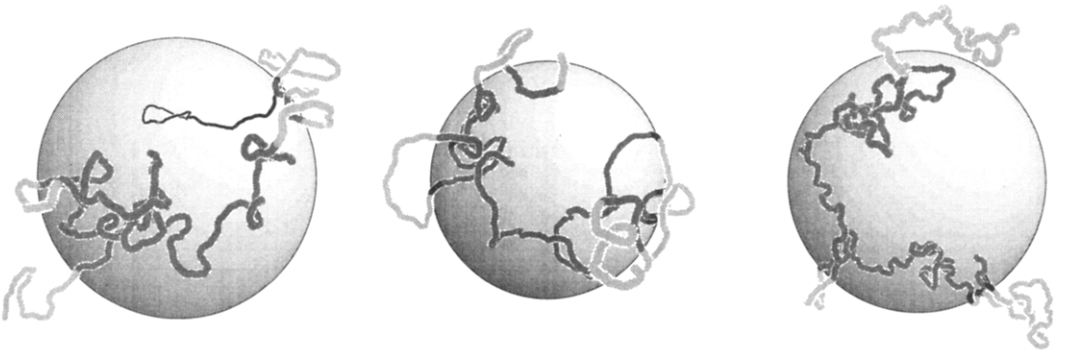

Figure 8. Representative instantaneous contours of HW Monte Carlo chains corresponding to the i- and a-PMMA and a-PS with $x = 500$ such that their radii of gyration S are just equal to their respective $\langle S^2\rangle^{1/2}$ (see the text).

details of the Monte Carlo method are given in Appendix B of ref 5. In Figure 8 are depicted representative instantaneous chain contours of these chains such that their radii of gyration S are just equal to the respective values of $\langle S^2\rangle^{1/2}$. The shaded sphere has the radius S, which is equal to 67.8, 57.4, and 63.2 Å for i-PMMA, a-PMMA, and a-PS, respectively, and is nearly proportional to $(\langle S^2\rangle/x_w)_\infty^{1/2}$ (see Figure 6). As expected from the above discussion, such distinguishable helical portions (each with almost one helix turn) as seen in the right bottom part of the picture for a-PMMA do not appear for i-PMMA. Thus the i-PMMA chain tends to take more extended conformations than the a-PMMA chain, so that the asymptotic ratio $(\langle S^2\rangle/x_w)_\infty$ is larger for the former despite the fact that λ^{-1} is smaller for the former. However, the chain contour of i-PMMA is still rather smooth compared to that of a-PS. This is due to the fact that λ^{-1} is larger for the former than for the latter. It is because of this (chain stiffness) that the ratio $(\langle S^2\rangle/x_w)_\infty$ is even larger for i-PMMA than for a-PS. (Note that the asymptotic ratio is smaller for a-PMMA than for a-PS because of the strong helical nature of the former.)

Concluding Remarks

The behavior of the ratio $\langle S^2\rangle/x_w$ as a function of x_w for the unperturbed i-PMMA with $f_r \simeq 0.01$ has been found to be remarkably different from that for the a-PMMA with $f_r = 0.79$ previously[5] studied. That is, it increases monotonically with increasing x_w and levels off to its asymptotic value for the former, while it exhibits a maximum for the latter. This difference arises from the fact that the i-PMMA chain is of weaker helical nature than the a-PMMA chain which retains rather large and clearly distinguishable helical portions in dilute solution. Such a dependence of the equilibrium conformational behavior of PMMA chains on the stereochemical composition f_r is considered to affect other dilute solution properties. Thus we proceed to study them in the forthcoming papers.

Acknowledgment. We thank Professor K. Hatada and Dr. K. Ute of Osaka University for their valuable advice about the polymerization of i-PMMA and also for their kind offer of unpublished ^{1}H NMR spectra for the stereochemical isomers of the MMA tetramer.

References and Notes

(1) Konishi, T.; Yoshizaki, T.; Shimada, J.; Yamakawa, H. *Macromolecules* **1989**, *22*, 1921 (see also succeeding papers).
(2) Yamakawa, H. *Annu. Rev. Phys. Chem.* **1984**, *35*, 23.
(3) Yamakawa, H. In *Molecular Conformation and Dynamics of Macromolecules in Condensed Systems*; Nagasawa, M., Ed.; Elsevier: Amsterdam, 1988; p 21.
(4) Flory, P. J. In *Statistical Mechanics of Chain Molecules*; Interscience: New York, 1969.
(5) Tamai, Y.; Konishi, T.; Einaga, Y.; Fujii, M.; Yamakawa, H. *Macromolecules* **1990**, *23*, 4067.
(6) Fujii, Y.; Tamai, Y.; Konishi, T.; Yamakawa, H. *Macromolecules* **1991**, *24*, 1608.
(7) Takaeda, Y.; Yoshizaki, T.; Yamakawa, H. *Macromolecules* **1993**, *26*, 3742.
(8) Yoshizaki, T.; Hayashi, H.; Yamakawa, H. *Macromolecules* **1993**, *26*, 4037.
(9) Dehara, K.; Yoshizaki, T.; Yamakawa, H. *Macromolecules* **1993**, *26*, 5137.
(10) Ute, K.; Asada, T.; Miyatake, N.; Hatada, K. *Makromol. Chem., Macromol. Symp.* **1993**, *67*, 147.
(11) Rubingh, D. N.; Yu, H. *Macromolecules* **1976**, *9*, 681.
(12) Berry, G. C. *J. Chem. Phys.* **1966**, *44*, 4550.
(13) Konishi, T.; Yoshizaki, T.; Saito, T.; Einaga, Y.; Yamakawa, H. *Macromolecules* **1990**, *23*, 290.
(14) Spěváček, J.; Schneider, B. *Makromol. Chem.* **1975**, *176*, 3409.
(15) Ute, K.; Nishimura, T.; Matsuura, Y.; Hatada, K. *Polym. J.* **1989**, *21*, 231.
(16) Ute, K.; Nishimura, T.; Hatada, K. *Polym. J.* **1989**, *21*, 1027; unpublished results.
(17) Chûjô, R.; Hatada, K.; Kitamura, R.; Kitayama, T.; Sato, H.; Tanaka, Y. *Polym. J.* **1987**, *19*, 413.
(18) Krause, S.; Cohn-Ginsberg, E. *J. Phys. Chem.* **1963**, *67*, 1479.
(19) Abe, F.; Einaga, Y.; Yamakawa, H. *Macromolecules* **1994**, *27*, 3262.
(20) Yamakawa, H. *Macromolecules* **1977**, *10*, 692.
(21) Abe, F.; Horita, K.; Einaga, Y.; Yamakawa, H. *Macromolecules* **1994**, *27*, 725.
(22) Yamakawa, H.; Fujii, M. *J. Chem. Phys.* **1976**, *64*, 5222.
(23) Kratky, O.; Porod, G. *Recl. Trav. Chim. Pays-Bas* **1949**, *68*, 1106.
(24) Abe, F.; Einaga, Y.; Yoshizaki, T.; Yamakawa, H. *Macromolecules* **1993**, *26*, 1884.
(25) Yamakawa, H.; Fujii, M. *J. Chem. Phys.* **1977**, *66*, 2584.
(26) Yamakawa, H.; Shimada, J.; Fujii, M. *J. Chem. Phys.* **1978**, *68*, 2140.